International Journal of Emerging Engineering and Technology (IJEET)
ISSN (e): 2958-3764
Volume: 4, Number:2, Pages: 20 -27, Year: 2025

Enhancing the Photocatalytic Performance of Anatase TiO_2 through Vanadium, Manganese and Nitrogen Do-doping: A DFT Study

Nauman Ahmad

Department of Physics, The University of Swabi, Khyber Pakhtunkhwa, Pakistan
Corresponding author: *Email addresses:* nauman5121go@gmail.com (Nauman Ahmad)

***Abstract*— TiO2 is a well-known photocatalyst with several potential applications. But because of its wider band gap, its optical activity is restricted to the UV region of the electromagnetic spectrum. These peak limits the photocatalytic activity of the specimen. To boost the photocatalytic activity of TiO2, it is necessary to shift its absorption peak from the ultraviolet to the visible range by reducing its bandgap. Doping of several metals and non-metals is one of the strategies adopted to decrease the bandgap of TiO2. This research article provides an overview of the effects of co-doping with Vanadium, Manganese, and Nitrogen on the structural and optoelectronic properties of anatase TiO2 using the framework of Density Functional Theory (DFT). V–N/TiO2, Mn–N/TiO2, and Mn–V/TiO2 were prepared, in which Mn and V were completely replaced at the i site, while N was at the O site. It was predicted that (V–N) doping in TiO2 decrease the bandgap from 2.13eV to 1.66eV. This decrease occurred due to the newly generated electronic states, i.e. V–3d and N–2p, below the conduction band minimum and the valence band maximum, respectively. (Mn– N) and (Mn–V) co-doping in TiO2 decrease the value of bandgap to 1.36eV and 1.22eV respectively. In these two models, the Fermi surface moved above the conduction band minimum, and thus, these models acted as N–type semiconductor. Co-doping also enhanced the optical performance of the specimen. It was observed that optical absorption increases as the model's bandgap energy decreases. The most enhanced optical absorption performance was predicted for Mn–V/TiO2 due to the effective electron-hole pair recombination.**

***Index Terms*— Anatase TiO_2, CASTEP Materials Studio, Density Functional Theory (DFT), photocatalysis, Fermi energy level, photoelectric conversion, electron-hole pair generation.**

I. Introduction

In recent years, Titanium Dioxide, also known as titania, a well-known transition metal oxide has gained the attention of potential researchers because of its promising characteristics such as optical and electronic properties[1], natural and geological availability, low cost and low toxicity[2] and high chemical and thermal stability[3]. Due to these unique characteristics, researchers are trying to utilize it for various technological advancements and applications, e.g., environmental cleanup such as air and water pollution[4], photo-catalytic water splitting for hydrogen production and storage[5], as electrode materials for super capacitors and energy storage[6], electronic and optoelectronic devices such as LEDs, Solar cells and nano sensors[2], and as an anti-reflection coating[7]. Since TiO_2 exhibits good optical and electrical properties, it can also be used as one of the promising semiconductors due to its effective utilization of the electron-hole pair.

Naturally, TiO_2 exists in three polymorphic states named Anatase, Brookite, and Rutile. Anatase is the metastable form of TiO_2 with a tetragonal crystal structure that is usually colorless or white in nature. Due to its potential applications, anatase TiO_2 is often prepared in the laboratory by chemical methods such as sol-gel route[8] through controlled hydrolysis of Titanium tetra-ethoxide ($Ti_4(OCH_2CH_3)_{16}$) [9] and titanium tetrachloride($TiCl_4$)[10]. Anatase TiO_2 has a space group of 141/AMD having the lattice constants as a = 3.776 Å, b = 3.776 Å , c = 9.486 Å.

Brookite is another polymorph of TiO_2 having orthorhombic geometry [11]. Brookite is a brittle mineral having reddish brown or deep red color. Brookite belongs to the space group of Pcba with lattice constants as a=5.4558 Å, b= 9.1819 Å. amd c= 5.1429 Å. having all three angles equals to 90. The formula mass for brookite is 79.88g/mol.

Rutile is the most common mineral oxide of TiO_2. Due to its high refractive index, it can be used in several optical instruments. It is thermodynamically the most stable polymorph than the other two. The unit cell of rutile is tetragonal having lattice constants a= 4.584 Å, b= 4.584 Å and c= 2.953 Å [12].

All the three polymorphs of TiO_2 shows good photocatalytic activity under UV radiation. But fundamental studies have revealed that the anatase is the most active polymorph than the other two forms due to the existence of reactive [001] face [13].

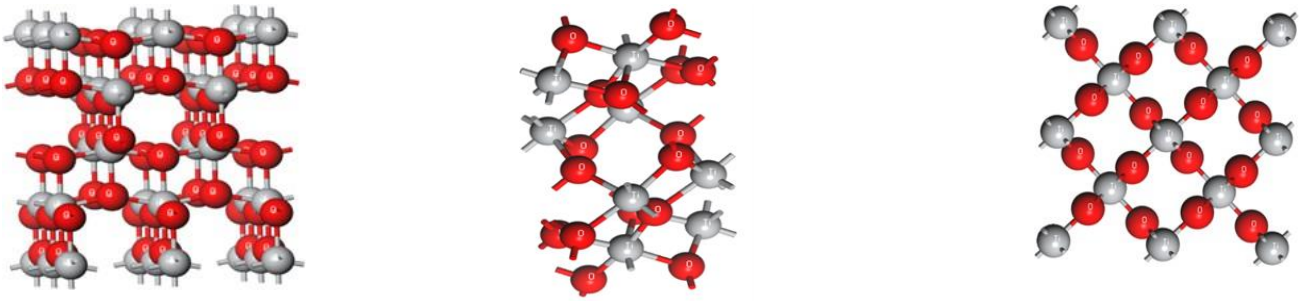

Figure 1: Structures of (a) Anatase (b) Brookite and (c) Rutile TiO_2

But this photocatalytic activity is subject to Ultra-Violet region of the solar irradiance only as the efficiency in the visible range is very low.

Rutile and anatase both have good photoconversion efficiency in Ultra-Voilet region but this efficiency is very low in Visible region. The high bandgap value of TiO2 is only reason behind this limitation. Experimentally, rutile and anatase have observed to have a bandgap value of 3.3 ± 0.5 eV [14] and 3.2 eV [13][15] respectively for k- points meshes of 9 x 9 x 3, 7 x 7 x 11 and 3 x 5 x 5 which corresponds to the optical absorption of solar light having wavelength less than 410nm and 390nm for rutile and anatase [16]. Moreover, pure TiO2 utilize the UV-light efficiently which contributes to only 4% of the total solar spectrum [15] [17] [18].

Furthermore, the performance of TiO2 is also limited due to the fast electron-hole pair recombination process. Enough energy is required for the electronic transitions within the bands and thus only light having more energy i.e. UV can be utilized [19]. Thus, it is necessary for the optical absorption peak to be shifted from UV region to Visible which contributed to about 45% of the electromagnetic spectrum [13] [18].

Several techniques have been developed to enhance the absorption peak from Ultra-Voilet region to the region of Visible spectrum. Amongst all the techniques, doping is one of the most common and useful method. Several metals such as Sulphur (S) [20] [21], Chromium (Cr) [22], Iron (Fe) [23], Molybdenum (Mo), Copper (Cu) [24] and Cobalt (Co) etc. and non-metals such as Nitrogen (N)[25] and Carbon (C)[26] are doped in TiO2 to reduce the bandgap an enhance visible light sensitivity. Metals and non-metals co-doping such as Ce–N [27], Fe—N [13] [28], Co–N [29] etc. and tri-doping such as In–Ag–N [30], Co–Mn–Fe [31] are also been calculated.

In this investigation, we showed the efficient photo-catalytic and optoelectronic properties of TiO2 through Manganese (Mn), Vanadium (V) and Nitrogen (N) co doping. Using the CAmbridge Serial Total Energy Package (CASTEP) code in Materials Studio, pure TiO2 and three co-doped models N–V/TiO2, N–Mn/TiO2, and V–Mn/TiO2 were pre- pared in which V, Mn are replaced at Ti position and N at O position. The N–2p energy level successfully fuses with the O–2p levels due to the comparable ionic sizes of Oxygen and Nitrogen, altering the electronic distribution of the valence band leading to the easily conduction of load carriers [32]. Due to the comparable ionic radii, all the three dopants (Mn, V, N) give least percent symmetry deviation resulting in the obtaining of least distorted co-doped models. All the models were then optimized geometrically using different regular k-points meshes and cutoff energy values. It was observed that the value of symmetry distortion was minimum at cutoff energy value of 400 eV and the centered k-point mesh of 3 x 3 x 2.

After the geometry optimization, using the Density Functional Theory (DFT) calculations, electronic properties like Band Structure and Density of States (total and partial) and Optical Properties were calculated. After the calculations, the opto-electronic properties were then compared graphically for the selection of best performing model.

II. Calculations

For all theoretical calculations, spin dependent Density Function Theory Calculations were performed utilizing CASTEP command of Material Studio, which uses pseudopotentials and plane wave basis sets. The following equation of Perdew–Burke–Ernzerhoff (PBE) exchange correlation function in the framework of Generalized Gradient Approximation (GGA) was used for all calculations.

The electronic wave function was extended in plane waves to a cut-off energy of 400 eV keeping the centered k-point mesh of 3x3x2 Monkhorst-Grid pack in the Brillouin zone. The pseudopotential option, which is the core- valence interaction, was set to Ultrasoft using Koelling-Harmon relativistic treatment. The unit cell of TiO_2 Anatase was extended to 2x2x1 supercell using the structural library of Materials Studio. Using the same parameters, a pure and three co-doped models were prepared where single Nitrogen (N), Manganese (Mn) and Vanadium (V) were substitutionally replaced at Oxygen and Titanium sites respectively as shown in the figure above.

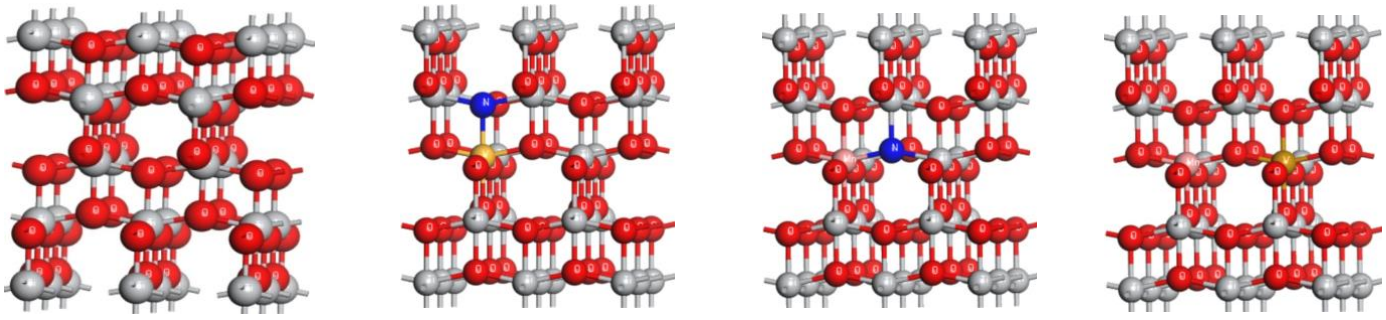

(a) (b) (c) (d)

Figure 2: 2 x 2 x 1 Supercells of Pure, N–V/TiO_2, N–Mn/TiO_2, and V–Mn/TiO_2 respectively

In order to get the most stable structures of all three models, their geometries were optimized by using Limited-memory Broydeen-Fletcher-Goldfard-Shanno (L-BFGS) algorithm from the family of quasi-Newton methods. The iterations were set to a maximum number of 100. All the models were converged by using displacement value of 0.002 Å, a maximum force of 0.05 eV/Å for total energy value of 2×10^{-5} eV⁄atom. The geometries of all models were optimized till the ground state electron density $\rho_{GS}(r)$ was computed from numerical method such as Kohn-Sham equation as:

$$\left[-\frac{\hbar^2}{2m_e}\nabla^2 + V_{ext}(r) + V_H(r) + V_{XC}(r)\right]\Psi(r) = E\Psi(r)$$

Where ε is the energy eigen values of the orbitals.

After solving the Kohn-Sham equation, the electron density can be calculated as;

$$\rho(r) = \sum_{i=1}^{n}|\Psi_i(r)|^2$$

The density is then used to update potentials, and the equation is solved again and again until true ground state electron density is computed which is called self-consistent field (SCF).

After geometry optimization, electronic band structure, band density of states (TDOS), and partial density of states (PDOS), as well as optical properties, were computed. When photons of appropriate energy interact with the electrons in the orbitals, the electrons get excited from the valence to the conduction band, corresponding to transitions from occupied to unoccupied states. Optical properties were derived from the calculated complex dielectric function. The electronic and optical characteristics of pure and co-doped models were then graphically compared for identification of the most efficient performing specimen.

III-Results and Discussions

3.1. Electronic Properties

3.1.1 Band Structure

Figure 3 shows the predicted diagrams of band structures of pure TiO_2, N–V/TiO_2, N–Mn/TiO_2, and V–Mn/TiO_2. The calculations were performed using Density Functional Theory (DFT) with a plane-wave cutoff energy of 400 eV and a $3 \times 3 \times 2$ k-point mesh. The pure TiO_2 was found to have a band gap of 2.13 eV, which is consistent with previously reported theoretical values such as 2.10 eV [2], 2.14 eV [33], 2.17 eV [34], 2.18 eV [35], 2.2 eV[36] and 2.21 eV [3].

In the N–V/TiO_2 doped TiO_2 system, Nitrogen (N) and Vanadium (V) were replaced at one Ti and one O site, respectively. This co-doping decreases the band gap to 1.65 eV. The narrowing originates by introducing N—2p acceptor states over the valence band maximum and V-–3d donor states just beneath the conduction band minimum. Although N—2p states act as electron-trapping recombination centers, the V—3d donors compensate by filling these traps. Consequently, the Fermi level does not shift significantly toward either band edge, and the (V-–N) system does not exhibit either p–type or n–type behavior.

For the (Mn-–N) doped TiO_2 configuration, the band energy value decreases further to 1.36 eV. In addition to N—2p states, Manganese generates donor states beneath the edge of the conduction band. The Mn substitution shifts the Fermi level toward the conduction band, resulting in n–type semiconducting behavior. The photocatalytic performance improves because Mn donors suppress the recombination associated with N-–2p trapping centers.

In the (Mn-–V) co-doped TiO_2 model, the band gap is significantly reduced to 1.22 eV. Both Mn and V contribute

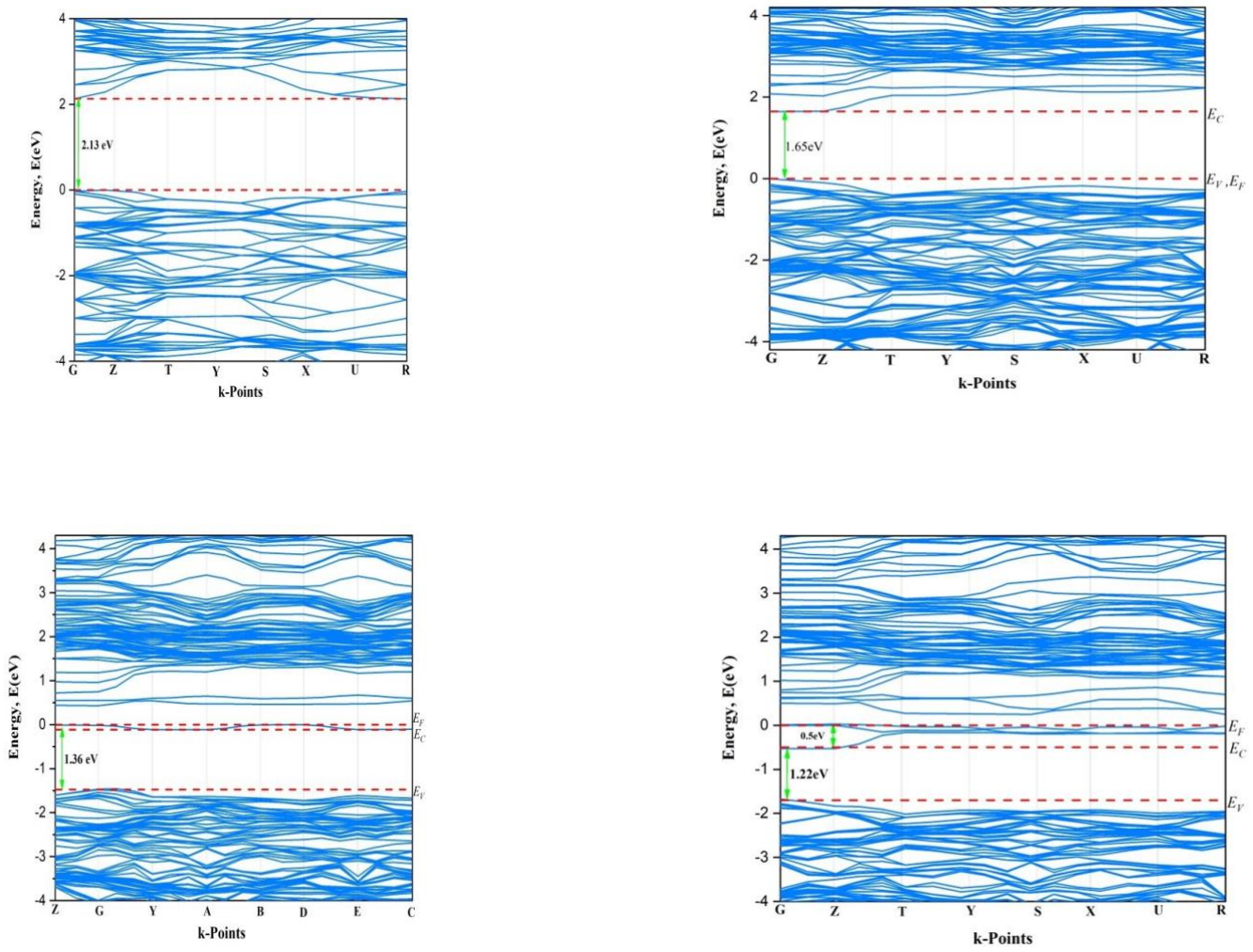

Figure 3: Theoretically Predicted Band Structures of Pure, V–N doped TiO_2, Mn–N doped TiO_2, and Mn–V doped TiO_2

donor states within the band energy gap beneath the edge of conduction band. Since, there was no nitrogen, no additional trapping centers were introduced, preventing recombination via N—2p levels. The combined effect of Mn and V doping shifts the Fermi level by approximately 0.5 eV above the conduction band minimum, confirming strong n–type character. The enhanced photocatalytic activity of this model is attributed to the time increment in recombining the photogenerated electron-–hole pairs.

3.1.2. Band Density of States

Figure 4 gives a comparative overview of the band density of states (TDOS) of TiO_2 and the three co-doped configurations. For pure TiO_2, a band gap of 2.13 eV is observed, with the Fermi energy level lies at the top of the valence band, reflecting intrinsic semiconducting behavior. The valence energy band is primarily comprises of O–2p levels, and the conduction band mainly comprises of Ti–3d orbitals.

When (V–N) is doped in TiO_2, the band energy value decreases to 1.65 eV. This narrowing is subjected to the introduction of N–2p acceptor states above valence band and V–3d donor states just beneath the conduction band minimum. Although these impurity levels modify the electronic structure, the Fermi energy level remains located at the valence band edge, predicting that the N–2p trapping centers have been filled by V–3d donor resulting in an intrinsic semiconductor behavior.

For the (Mn–N) co-doped configuration, band energy value decreases further to 1.36 eV. In this configuration, Mn introduces additional donor states within the band gap down the conduction band minimum, shifting the Fermi level slightly toward the conduction band. The combined presence of Mn–3d donor states and N–2p acceptor states en- hances visible-light absorption and reduces recombination by partially neutralizing the N–2p trapping centers, thereby improving the photocatalytic activity.

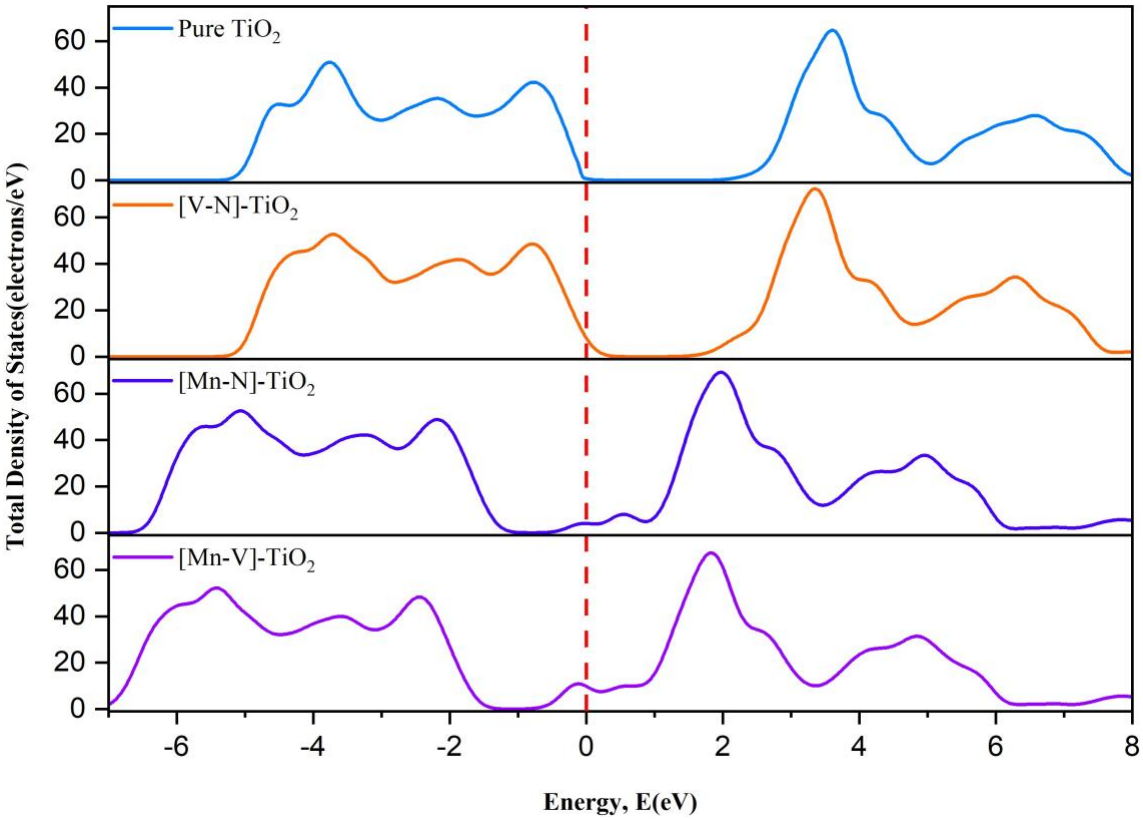

Figure 4: Band Density of States Comparison for Pure and Doped TiO_2 Models

In the (Mn–V) co-doped TiO_2 structure, the band gap reaches its minimum value of 1.22 eV. Both Mn and V introduce donor energy levels down the conduction band edge, significantly reducing the band gap and shifting the Fermi level upward. Since no nitrogen is involved this time, no new carrier trapping states are formed, which reduces electron–hole recombination pathways. Consequently, this model exhibits enhanced n-type behavior and improved photocatalytic performance due to better charge carrier separation.

Overall, the DOS analysis suggests that co-doping TiO_2 with transition metals and nonmetals effectively refines the electronic symmetry by making the band width narrower and introducing new impurity states, therefore enhancing visible-light-driven photocatalytic performance.

3.1.3. Partial Density of States

Partial density of states (PDOS) peaks for pure model of TiO_2 is shown on the figure 5(a). The plot suggests that the valence energy band comprises of O–2p states, whereas the conduction energy band consists of Ti–3d states. This distribution reflects the intrinsic electronic nature of TiO_2, with a wide value of band gap energy of 2.13 eV.

Figure 5(b) illustrates the PDOS of (N–V) co-doped TiO_2

Vanadium introduces V–3d donor levels near the conduction band edge. Similarly, Nitrogen generates N–2p acceptors near the edge of valence energy band. Introduction of these new impurity states results in reducing the band gap from 2.13 eV to 1.65 eV.

Figure 5(c) shows the PDOS of the (Mn–N) co-doped configuration. Both Mn–3d and N–2p impurity states appear inside the band gap; however, the peak of Mn–3d is more dominant than that of N–2p, indicating a dominant Mn contribution to band-gap narrowing. As a result, the band gap decreases to 1.36 eV. The strong donor behavior of Mn–3d states shifts the Fermi surface toward the conduction energy band, giving (Mn–N) model a clear n-type semiconducting behavior.

Finally, Figure 5(d) illustrates the PDOS of the Mn–V/TiO_2. Both Manganese and Vanadium generate donor 3d states below the bottom level of the conduction energy band, significantly narrowing the band gap from 2.13 eV to 1.22 eV. The intrinsic Fermi surface shifts upward by approximately 0.5 eV into the conduction band due to the generation of these new energy level. Consequently, the (Mn–V) co-doped structure exhibits strong n-type semiconducting characteristics.

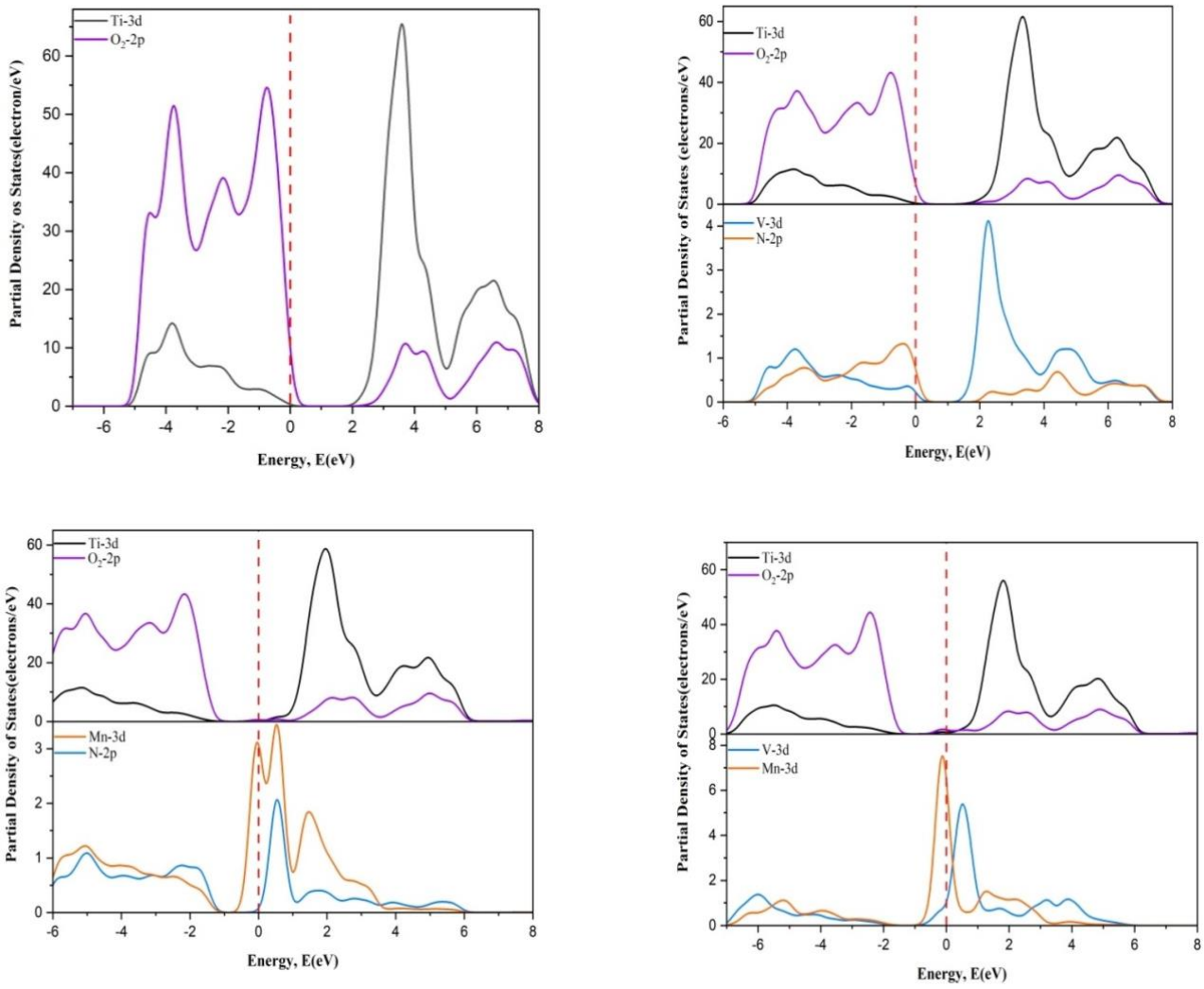

Figure 5: Partial Density of States peaks of (a) Pure, (b) V–N doped TiO_2, (c) Mn–N doped TiO_2, and (d) Mn–V doped TiO_2

3.2. Optical Properties

Figure 6 presents the mutual comparison of predicted photo-absorption spectra of TiO_2 and its doped models. For pure TiO_2, the band gap is 2.13 eV, indicating that electrons should have 2.13 eV energy for transition from the O–2p level (valence band) to the Ti–3d level (conduction band). Such a large band gap limits absorption primarily to the region of ultraviolet (UV) spectrum. The figure clearly demonstrates that introducing external impurities into TiO_2 shifts the absorption peak toward the visible region, which covers nearly 45% of the solar spectrum, thereby enhancing its photocatalytic potential.

A comparison of the absorption spectra shows that all co-doped models exhibit improved absorption relative to pure TiO_2. In the (V–N) co-doped system, the absorption is only slightly enhanced. This slight enhancement arises because the number of donor states introduced by Vanadium are partially reduces by the N–2p acceptor states, which act as trapping centers and hinder significant absorption.

Similarly, (Mn–N) doped model shows stronger absorption in the visible region. This is attributed to the dominant contribution of Mn–3d donor states, which dominates the trapping effect associated with N–2p states and allows more efficient electronic excitation. Consequently, (Mn–N) TiO_2 exhibits a higher absorption intensity than both the pure and the (V–N) models.

For the (Mn–V) co-doped TiO_2, both Vanadium and Manganese generate donor states without generating new trap centers. As a result, all donor contributions effectively enhance photon absorption across the visible range. The absorption curve for (Mn–V)/TiO_2 remains consistently high with increasing wavelength, unlike the other models whose absorption intensity decreases when the wavelength increases to the visible region of the solar spectrum. This behavior

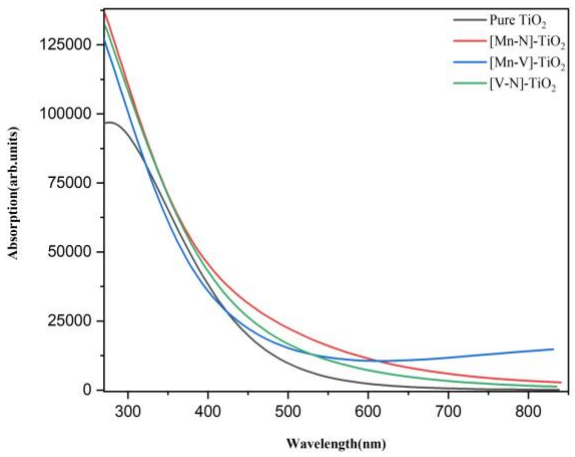

Figure 6: Optical Absorption Spectra comparison of Pure and other doped TiO_2

originates from the significantly reduced band gap value to 1.22 eV and the absence of carriers trapping centers, as found in the other two systems.

Overall, the (Mn–V) co-doped TiO_2 model exhibits the most pronounced improvement in optical absorption, indicating excellent photocatalytic performance for both UV and visible-region.

IV. Conclusion

In this article, we carried out Density Functional Theory (DFT) calculations to show the effect of co-doping on the optoelectronic properties of anatase TiO_2. Four models were considered: Pure, V–N/TiO_2, Mn–N/TiO_2, and Mn–V/TiO_2, which were prepared using structural library of Materials Studio. Electronic properties, such as band structure and density of states, as well as optical absorption spectra, were calculated for each model. The band gap values were predicted to be 2.13 eV, 1.65 eV and 1.36 eV for pure TiO_2, (N–V) doped TiO_2 and (N–Mn) doped TiO_2 respectively with the smallest band gap of 1.22 eV predicted for (Mn–V) doped TiO_2. Analysis of the optical properties revealed that the (V–Mn) co-doped model exhibits the more efficient optical absorption among all the studied systems, indicating its potential for photocatalytic applications.

FUNDING STATEMENT

The author(s) received no specific funding for this study.

CONFLICTS OF INTEREST

The authors declare no conflicts of interest to report regarding the present study.

INSTITUTIONAL REVIEW BOARD STATEMENT

Not applicable.

INFORMED CONSENT STATEMENT

Not applicable.

DATA AVAILABILITY STATEMENT

Data is available on reasonable request.

REFERENCES

[1] W. Zeng, T. Liu, Z. Wang, S. Tsukimoto, M. Saito, Y. Ikuhara, Oxygen adsorption on anatase tio2 (101) and (001) surfaces from first principles, Materials transactions 51 (1) (2010) 171–175.

[2] J. K. Mbae, Z. W. Muthui, Ab initio investigation of the structural and electronic properties of alkaline earth metal-tio2 natural polymorphs, Advances in Materials Science and Engineering 2022 (1) (2022) 7629651.

[3] Y. Wang, R. Zhang, J. Li, L. Li, S. Lin, First-principles study on transition metal-doped anatase tio 2, Nanoscale research letters 9 (2014) 1–8.

[4] X. Kang, S. Liu, Z. Dai, Y. He, X. Song, Z. Tan, Titanium dioxide: from engineering to applications, Catalysts 9 (2) (2019) 191.

[5] G. C. Va´squez, D. Maestre, A. Cremades, J. Ram´ırez-Castellanos, E. Magnano, S. Nappini, S. Z. Karazhanov, Understanding the effects of cr doping in rutile tio2 by dft calculations and x-ray spectroscopy, Scientific reports 8 (1) (2018) 8740.

[6] R. Lakra, R. Kumar, S. kumar, D. Thatoi, A. Soam, Synthesis of tio2 nanoparticles as electrodes for supercapacitor, Materials Today: Proceedings 74 (2023) 863–866, 3rd International Conference on Recent Advances in Mechanical Engineering Research and Development. doi:https://doi.org/10.1016/j.matpr.2022.11.271.
URL: https://www.sciencedirect.com/science/article/pii/S2214785322071222X

[7] J.-Y. Wang, C.-S. Huang, S.-L. Ou, Y.-S. Cho, J.-J. Huang, One-step preparation of tio2 anti-reflection coating and cover layer by liquid phase deposition for monocrystalline si perc solar cell, Solar Energy Materials and Solar Cells 234 (2022) 111433. doi:https://doi.org/10.1016/j.solmat.2021.111433.
URL: https://www.sciencedirect.com/science/article/pii/S092702482100474 8

[8] A. Swaminathen, D. Kumar, B. Ashok Kumar, P. Venugopal, S. Kathirvel, M. Kuttimarks, Evaluation of synthesis of tio2 nanoparticles via solgel method using acetone, Materials Today: Proceedings (2024). doi:https://doi.org/10.1016/j.matpr.2024.05.012.
URL: https://www.sciencedirect.com/science/article/pii/S2214785324003079

[9] K. D. Kim, H. T. Kim, Synthesis of tio2 nanoparticles by hydrolysis of teot and decrease of particle size using a two-stage mixed method, Powder Technology 119 (2) (2001) 164–172. doi:https://doi.org/10.1016/S0032-5910(00)00420-4.
URL: https://www.sciencedirect.com/science/article/pii/S0032591000004204

[10] T.-H. Wang, A. Navarrete-Lo´pez, S. Li, D. Dixon, J. Gole, Hydrolysis of ticl4: Initial steps in the production of tio2, The journal of physical chemistry. A 114 (2010) 7561–70. doi:10.1021/jp102020h.

[11] M. H. Samat, M. F. M. Taib, O. H. Hassan, M. Z. A. Yahya, A. M. M. Ali, Structural, electronic and optical properties of brookite phase titanium dioxide, Materials Research Express 4 (4) (2017) 044003. doi:10.1088/2053-1591/aa67b3.
URL: https://doi.org/10.1088/2053-1591/aa67b3

[12] D. A. Hanaor, W. Xu, M. Ferry, C. C. Sorrell, Abnormal grain growth of rutile tio2 induced by zrsio4, Journal of Crystal Growth 359 (2012) 83–91. doi:https://doi.org/10.1016/j.jcrysgro.2012.08.015.
URL: https://www.sciencedirect.com/science/article/pii/S0022024812005672

[13] C. Thambiliyagodage, S. Mirihana, Photocatalytic activity of fe and cu co-doped tio2 nanoparticles under visible light, Journal of Sol-Gel Science and Technology 99 (1) (2021) 109–121.

[14] M. Landmann, E. Rauls, W. Schmidt, The electronic structure and optical response of rutile, anatase and brookite tio 2, Journal of physics. Condensed matter : an Institute of Physics journal 24 (2012) 195503. doi:10.1088/0953-8984/24/19/195503.

[15] T. Wang, T. Xu, Effects of vanadium doping on microstructures and

optical properties of tio2, Ceramics International 43 (1, Part B) (2017) 1558–1564. doi:https://doi.org/10.1016/j.ceramint.2016.10.132.

[16] F. Amano, A. Yamamoto, J. Kumagai, Highly active rutile tio2 for photocatalysis under violet light irradiation at 405 nm, Catalysts 12 (10) (2022) 1079.

[17] E. Shin, S. Jin, J. Kim, S.-J. Chang, B.-H. Jun, K.-W. Park, J. Hong, Preparation of k-doped tio2 nanostructures by wet corrosion and their sunlight-driven photocatalytic performance, Applied Surface Science 379 (2016) 33–38. doi:https://doi.org/10.1016/j.apsusc.2016.03.222.

[18] Q. Xiao, Z. Si, Z. Yu, G. Qiu, Sol–gel auto-combustion synthesis of samarium-doped tio2 nanoparticles and their photocatalytic activity under visible light irradiation, Materials Science and Engineering: B 137 (1-3) (2007) 189–194.

[19] S. Douven, J. G. Mahy, C. Wolfs, C. Reyserhove, D. Poelman, F. Devred, E. M. Gaigneaux, S. D. Lambert, Efficient n, fe co-doped tio2 active under cost-effective visible led light: from powders to films, Catalysts 10 (5) (2020) 547.

[20] T. Ohno, T. Mitsui, M. Matsumura, Photocatalytic activity of s-doped tio2 photocatalyst under visible light, Chemistry letters 32 (4) (2003) 364–365.

[21] T. Umebayashi, T. Yamaki, S. Tanaka, K. Asai, Visible light-induced degradation of methylene blue on s-doped tio2, Chemistry letters 32 (4) (2003) 330–331.

[22] S. Klosek, D. Raftery, Visible light driven v-doped tio2 photocatalyst and its photooxidation of ethanol, The Journal of Physical Chemistry B 105 (14) (2001) 2815–2819.

[23] J. Yu, H. Yu, C. Ao, S. Lee, J. C. Yu, W. Ho, Preparation, characterization and photocatalytic activity of in situ fe-doped tio2 thin films, Thin Solid Films 496 (2) (2006)273–280. doi:https://doi.org/10.1016/j.tsf.2005.08.352.
URL: https://www.sciencedirect.com/science/article/pii/S0040609005015713

[24] J. Choi, H. Park, M. R. Hoffmann, Effects of single metal-ion doping on the visible-light photoreactivity of tio2, The Journal of Physical Chemistry C 114 (2) (2010) 783–792.

[25] R. Nakamura, T. Tanaka, Y. Nakato, Mechanism for visible light responses in anodic photocurrents at n-doped tio2 film electrodes, The Journal of Physical Chemistry B 108 (30) (2004) 10617–10620.

[26] G. Liu, C. Han, M. Pelaez, D. Zhu, S. Liao, V. Likodimos, N. Ioannidis, A. G. Kontos, P. Falaras, P. S. Dunlop, et al., Synthesis, characterization and photocatalytic evaluation of visible light activated c-doped tio2 nanoparticles, Nanotechnology 23 (29) (2012) 294003.

[27] M. Nasir, S. Bagwasi, Y. Jiao, F. Chen, B. Tian, J. Zhang, Characterization and activity of the ce and n co-doped tio2 prepared through hydrothermal method, Chemical Engineering Journal 236 (2014) 388–397.

[28] X. Yang, C. Cao, L. Erickson, K. Hohn, R. Maghirang, K. Klabunde, Photo-catalytic degradation of rhodamine b on c-, s-, n-, and fe-doped tio2 under visible-light irradiation, Applied Catalysis B: Environmental 91 (3-4) (2009) 657–662.

[29] L. Zhang, X. Li, Z. Chang, D. Li, Preparation, characterization and photoactivity of hollow n, co co-doped tio2/sio2 microspheres, Materials science in semiconductor processing 14 (1) (2011) 52–57.

[30] M. Khan, Y. Zeng, Improving the photo-response of tio2 by tri-doping: a dft based atomistic study, Materials Research Express 6 (11) (2019) 115510. doi:10.1088/2053-1591/ab46cc.
URL: https://doi.org/10.1088/2053-1591/ab46cc

[31] A. Youssef, S. Yakout, Mono, dual and tri-doped tio2: Sunlight photocatalytic, room temperature ferromagnetic and dielectric constant properties, Materials Chemistry and Physics 282 (2022) 125978. doi:https://doi.org/10.1016/j.matchemphys.2022.125978.
URL: https://www.sciencedirect.com/science/article/pii/S02540584 2200284X

[32] A. Realpe Jimenez, D. Nunez, N. Rojas, Y. Ramirez, M. Acevedo, Effect of fe–n codoping on the optical properties of tio2 for use in photoelectrolysis of water, ACS omega 6 (7) (2021) 4932–4938.

[33] Z. Lin, A. Orlov, R. M. Lambert, M. C. Payne, New insights into the origin of visible light photocatalytic activity of nitrogen-doped and oxygen-deficient anatase tio2, The journal of physical chemistry B 109 (44) (2005) 20948–20952.

[34] S.-D. Mo, W. Ching, Electronic and optical properties of three phases of titanium dioxide: Rutile, anatase, and brookite, Physical review B 51 (19) (1995) 13023.

[35] M. Guo, J. Du, First-principles study of electronic structures and optical properties of cu, ag, and au-doped anatase tio2, Physica B: Condensed Matter 407 (6) (2012) 1003–1007.

[36] S. Sudarsono, N. K. Salsabila, R. Asih, G. Yudoyono, D. Darminto, Optical properties of anatase tio2: Computational and experimental studies, AIP Conference Proceedings 2604 (2023) 070005. doi:10.1063/5.0116780.
URL : https://doi.org/10.1063/5.0116780